

# Bayesian cosmological inference through implicit cross-correlation statistics

G. Lavaux<sup>1</sup> and J. Jasche<sup>2</sup>

<sup>1</sup> Institut d'Astrophysique de Paris (IAP), CNRS & Sorbonne Université, UMR 7095, 98 bis bd Arago, F-75014 Paris, France  
e-mail: guilhem.lavaux@iap.fr

<sup>2</sup> The Oskar Klein Centre, Department of Physics, Stockholm University, AlbaNova University Centre, SE 106 91 Stockholm, Sweden  
e-mail: jens.jasche@fysik.su.se

April 28, 2021

## ABSTRACT

*Context.* Analyses of next-generation galaxy data require accurate treatment of systematic effects such as the bias between observed galaxies and the underlying matter density field. However, proposed models of the phenomenon are either numerically expensive or too inaccurate to achieve unbiased inferences of cosmological parameters even at mildly-nonlinear scales of the data.

*Aims.* As an alternative to constructing accurate galaxy bias models, requiring understanding galaxy formation, we propose to construct likelihood distributions for Bayesian forward modeling approaches that are insensitive to linear, scale-dependent bias and provide robustness against model misspecification.

*Methods.* We use maximum entropy arguments to construct likelihood distributions designed to account only for correlations between data and inferred quantities. By design these correlations are insensitive to linear galaxy biasing relations, providing the desired robustness. The method is implemented and tested within a Markov Chain Monte Carlo approach. The method is assessed using a halo mock catalog based on standard full, cosmological,  $N$ -body simulations.

*Results.* We obtain unbiased and tight constraints on cosmological parameters exploiting only linear cross-correlation rates for  $k \leq 0.10h \text{ Mpc}^{-1}$ . Tests for halos of masses  $\approx 10^{12}h^{-1} M_{\odot}$  to  $\approx 10^{13}h^{-1} M_{\odot}$  indicate that it is possible to ignore all details of the linear, scale dependent, bias function while obtaining robust constraints on cosmology. Our results provide a promising path forward to analyses of galaxy surveys without the requirement of having to accurately model the details of galaxy biasing but by designing robust likelihoods for the inference.

**Key words.** (cosmology:) large-scale structures of Universe – (cosmology:) cosmological parameters – methods: statistical – methods: numerical – methods: data analysis

## 1. Introduction

Cosmological analyses of next-generation galaxy surveys will no longer be limited by observational uncertainties but by our ability to handle systematic effects of the data. A particular nuisance in inferring cosmological parameters from galaxy clustering data is the unknown biasing relation between observed galaxies and the underlying matter distribution. Available galaxy bias models are either numerically complex or too inaccurate for inferences at mildly non-linear and non-linear scales. The problem becomes more severe when realizing that accurate statistical inference also requires choosing a likelihood distribution, describing the statistical generation of the observations, typically galaxy counts, given a model. It is now realized that unbiased, high precision inference of next generation observations requires control on the accuracy of the data model that we currently do not have (van Daalen et al. 2011; Schneider et al. 2019; van Daalen et al. 2020, e.g). The canonical approach is to use ever more complex simulation models introducing additional nuisance parameters to arrive at sufficiently expressive data models that yield unbiased cosmological inferences (e.g. for power spectrum Smith et al. 2003; Mead et al. 2015). These nuisance parameters are of no immediate interest and will have to be marginalized out under significant numerical costs (e.g. for weak lensing Hildebrandt et al. 2017).

Here-above, we are already assuming that the fundamental data set is provided by observation of galaxies broadly classified by their sky position and luminosity, which is the typical procedure for galaxy clustering analysis. We then form galaxy counts on a mesh, which is itself another summary statistics. This statement is at odd with principled approached of likelihood analysis which must provides realization of the fundamental data set and not of its summaries, particularly if the summaries are not sufficient. No “likelihood” probability function for galaxy counts which accounts for marginalized over all possible small scale physics, including missing cosmological fluctuations at very small scales, has been derived so far.

Recently an alternative has been proposed to use effective field theory to derive from first principles and by a well-defined series expansion an accurate data model of galaxy field on large scales to infer cosmological information from observations (Schmidt et al. 2019; Elsner et al. 2020; Cabass & Schmidt 2020; Schmidt et al. 2020; Schmidt 2021). This offers a principled approach to the control of the bias expansion that is physically achievable.

The present work is part of a series of papers attempting to investigate a different idea. Instead of constructing over-parametrized models to explain the data and marginalize out nuisance parameters, we aim to direct construct likelihood distribu-

tions that are robust to data model misspecifications. To achieve this goal we will use Maximum Entropy principles to construct a robust likelihood that reduces the requirement of exactly predicting the data to satisfying only constraints on the cross-correlation between the data and inferred quantities.

Cross-correlation, or directional statistics, is a powerful approach to remove noise in various astronomical and cosmological applications. For example, the characterization of integrated Sachs Wolf effect (Granett et al. 2008), the Cosmic Infrared Background (e.g Elbaz et al. 2002; Planck Collaboration et al. 2014) or gravitational lensing (Smith et al. 2007). Some aspects of the idea of directional statistics coupled with wavelets has been found to be powerful for generating quickly and analyze non-Gaussian fields for cosmological parameters through adequate compression (Allys et al. 2020).

In this work, we seek to infer matter density fields implicitly through cross-correlation by designing a likelihood that reproduces the essential features of a physical model up to a certain scale. We will test the reliability of the proposed likelihood on halo mock data derived from specific  $N$ -body simulations. To assess the success of this test we infer the value of  $\sigma_8$ , which constrain the amplitude of the primordial power spectrum of adiabatic scalar fluctuations.

This article is organized as follows. In Section 2, we design the new likelihood. In Section 3, we precise what is the adopted cross-correlation model for large scale structures. In Section 4, we run self-consistent tests to check the accuracy of the algorithms. We test in Section 5 the likelihood in an unfavorable situation with halos provided from full, pure dark matter,  $N$ -body simulations. We give our conclusions in Section 6.

## 2. Building a cross-correlation likelihood

In this section, we build a mathematical tool based on directional statistics, specifically the von Mises-Fisher distribution, to construct likelihoods for cosmological analyses and discuss their properties (Fisher 1953).

### 2.1. Motivation

The use of galaxy clustering data fundamentally assumes that galaxy number counts correlate with matter density. This assumption has been extensively tested in observations and simulations in many past works. It has been noted that, while it holds on average, the exact relation between dark matter and cosmological objects such as halo and galaxies introduces is scale-dependent (Smith et al. 2007; Beutler et al. 2017). This scale dependence, affecting scales  $k > 0.05h \text{ Mpc}^{-1}$ , is subject to concerns as it hinders the reliable extraction of cosmological information from data. We intend to investigate ways to circumvent the problem. Notably, in the absence of a detailed model of galaxy formation, model-independent statistical correlations, or associations may be promising approaches to explore cosmology with galaxy surveys.

The relation between the dark matter field and the distribution of tracers is even more crucial for Bayesian forward modeling approaches, such as BORG (Jasche & Wandelt 2013; Jasche & Lavaux 2019), which relies on our capability to model fairly accurately the observational signal. A solution to this conundrum can be provided by a likelihood that is sensitive only to the cross-correlation between matter density and galaxy number counts but not to the exact absolute mapping between the two. We can push even further: we can request that this cross-correlation oc-

curs at a different rate for very fine bins of Fourier mode amplitude. For the sake of simplicity, we will limit ourselves in this work to linear cross-correlation between two fields.

We will simplify the design for now by considering a very fine bin  $k$ , defined by the set  $B_k = \{\mathbf{k} \mid k \leq |\mathbf{k}| < k + \Delta k\}$ , and consider the cross-correlation product  $C(k)$  between the deterministic field  $\delta$  and the observed field  $N$ . In discrete Fourier representation, that relation is:

$$C(k) = \sum_{\mathbf{k} \in B_k} \hat{\delta}^*(\mathbf{k}) \hat{N}(\mathbf{k}) = \mathbf{V}_\delta^k \cdot \mathbf{V}_N^k, \quad (1)$$

with  $\mathbf{V}_a^q$  ( $a$  being  $\hat{\delta}$  or  $\hat{N}$ ) a vector in a high dimensional space (determined by the size of  $B_k$  and other symmetric properties of  $\hat{\delta}$  and  $\hat{N}$ ) such that the components take the values from  $a$ . To simplify the discussion for the moment, we may just set each component as  $(\mathbf{V}_a^q)_i = a(\mathbf{q}_i)$ , where  $a \in \{\hat{\delta}, \hat{N}\}$ . However, we must keep in mind that the act of transforming  $a$  into  $\mathbf{V}_a$  may involve taking real and imaginary part and discarding the hermitically conjugate parts. Assuming that the fields must satisfy isotropy then we may express the first constraint that we are seeking for the likelihood is

$$\left\langle \frac{C(k)}{|\mathbf{V}_\delta^k| |\mathbf{V}_N^k|} \right\rangle = r(k), \quad (2)$$

with  $r(k)$  the correlation rate in the bin  $k$ . This function  $r(k)$  is not expected to depend strongly anymore on  $\delta$  or  $N$ , though that will need be tested in the future.

Thus, the sought probability distribution function  $\mathcal{P}(\mathbf{x}|\boldsymbol{\mu})$ , with  $\mathbf{x}$  the stochastic observed field (here  $N$ ) and  $\boldsymbol{\mu}$  the model field (here  $\delta$ ), satisfies the constraint:

$$\langle \mathbf{x} \cdot \boldsymbol{\mu} \rangle_{\mathcal{P}(\mathbf{x}|\boldsymbol{\mu}, \eta)} = \eta. \quad (3)$$

Here-above, without loss of generality, we have taken  $|\mathbf{x}| = 1$  and  $|\boldsymbol{\mu}| = 1$ . Furthermore, to link with the cosmological problem,  $\eta$  is equal for each bin to  $r(k)$ . Looking for the distribution that maximize the entropy while satisfying that constraint lead to the following function to optimize:

$$S = - \int d\Omega(\mathbf{x}) \mathcal{P}(\mathbf{x}|\boldsymbol{\mu}) \log(\mathcal{P}(\mathbf{x}|\boldsymbol{\mu})) + \lambda \left( \int d\Omega(\mathbf{x}) \mathcal{P}(\mathbf{x}|\boldsymbol{\mu}, \eta) - 1 \right) + \kappa \left( \int d\Omega(\mathbf{x}) \mathcal{P}(\mathbf{x}|\boldsymbol{\mu}, \eta) (\mathbf{x} \cdot \boldsymbol{\mu}) - \eta \right), \quad (4)$$

where the integration is done over the unit sphere in  $D$  dimensions corresponding to the vector space to which belongs  $\mathbf{a}$ . The constraint linked to the Lagrange multiplier  $\lambda$  serves to enforce normalization, while the constraint linked  $\kappa$  enforces the mean of the correlation. This maximization leads to:

$$\mathcal{P}(\mathbf{x}|\boldsymbol{\mu}, \eta) \propto \exp(\kappa(\eta) \mathbf{x} \cdot \boldsymbol{\mu}). \quad (5)$$

Up to the proportionality constant that can be obtained by enforcing a unit-normalization to the probability distribution. This function is the von Mises-Fisher (VMF) distribution (Fisher 1953), which we investigate further in Section 2.2. Before moving on, we note a peculiarity of this likelihood: it requires a non-linear combination of the amplitude of Fourier modes on a sphere of constant  $k$ . As such, it is non-local both in Fourier and in real representation. We have investigated some analytical properties of the variance of that likelihood for different correlation rates.

## 2.2. The von Mises-Fisher distribution

The von Mises-Fisher (VMF) distribution is defined on the unit sphere  $\mathbf{S}_p$  in  $p$  dimensions:

$$f_p(\mathbf{x} | \boldsymbol{\mu}, \kappa) = C_p(\kappa) \exp(\kappa \mathbf{x} \cdot \boldsymbol{\mu}), \quad (6)$$

where  $\kappa$  is a parameter,  $\boldsymbol{\mu}$  is the mean direction pointed by the distribution, and  $C_p(\kappa)$  is normalization of the distribution. It can be shown (Sra 2007) that the normalization has the following form:

$$C_p(\kappa) = \frac{\kappa^{p/2-1}}{(2\pi)^{p/2} I_{p/2-1}(\kappa)}, \quad (7)$$

with  $I_\nu(\kappa)$  the modified Bessel function of the first kind. To relate the coefficient  $\kappa$  to the correlation rate  $\langle \hat{\delta}^\dagger \hat{N} \rangle$ , we need to compute the first moment of the VMF distribution:

$$Q(\kappa) = \langle \mathbf{x} \cdot \boldsymbol{\mu} \rangle = \int_{\mathbf{S}_p} d\Omega(\mathbf{x}) (\mathbf{x} \cdot \boldsymbol{\mu}) C_p(\kappa) \exp(\kappa \mathbf{x} \cdot \boldsymbol{\mu}). \quad (8)$$

Now this can be obtained by noticing that:

$$\overline{Q_p(\kappa)} = C_p(\kappa) \frac{d}{d\kappa} \int_{\mathbf{S}_p} d\Omega(\mathbf{x}) \exp(\kappa \mathbf{x} \cdot \boldsymbol{\mu}). \quad (9)$$

Moreover the distribution satisfies the identity, which means:

$$\frac{d}{d\kappa} \left( C_p(\kappa) \int_{\mathbf{S}_p} d\Omega(\mathbf{x}) \exp(\kappa \mathbf{x} \cdot \boldsymbol{\mu}) \right) = 0, \quad (10)$$

which leads to

$$\frac{d}{d\kappa} \int_{\mathbf{S}_p} d\Omega(\mathbf{x}) \exp(\kappa \mathbf{x} \cdot \boldsymbol{\mu}) = -\frac{1}{C_p(\kappa)} \frac{dC_p}{d\kappa} = -\frac{d \log C_p}{d\kappa}. \quad (11)$$

Thus the equation satisfied by  $Q_p(\kappa)$  is:

$$Q_p(\kappa) = -\frac{d \log C_p}{d\kappa} = \frac{I'_{p/2-1}(\kappa)}{I_{p/2-1}(\kappa)} - \left( \frac{p}{2} - 1 \right) \log \kappa \quad (12)$$

$$= \frac{I_{p/2+1}(\kappa)}{I_{p/2-1}(\kappa)}. \quad (13)$$

We can now derive the relation between  $\kappa$  and the mean correlation between the unit vectors  $\mathbf{V}_\delta^{(i)} = \{\hat{\delta}(\mathbf{k}) | \mathbf{k} \in B_i\}$  and  $\mathbf{V}_N^{(i)} = \{\hat{N}(\mathbf{k}) | \mathbf{k} \in B_i\}$ :

$$\left\langle \sum_j \mathbf{V}_\delta^{(i)} \mathbf{V}_N^{(i)} \right\rangle = r(k_i). \quad (14)$$

The identities in Equations (9) and (13) leads to a consistency equation in  $\kappa$

$$r(k_i) = \frac{I_{p_i/2+1}(\kappa)}{I_{p_i/2-1}(\kappa)}, \quad (15)$$

with  $p_i = |B_i|$  the number of independent Fourier modes in the bin  $i$ , and  $r(\kappa)$  is the correlation rate introduced in Equation (2). We show in Figure 1 the relation for different values of  $p$ , the number of dimensions which is related to the bin size.

As we can see, the variance is a derived quantity for this distribution, contrary to the Gaussian distribution for which it can be further imposed. We will thus now compute it for a given value of the  $\kappa$  parameter. The definition of the variance  $V_p(\kappa)$ , for

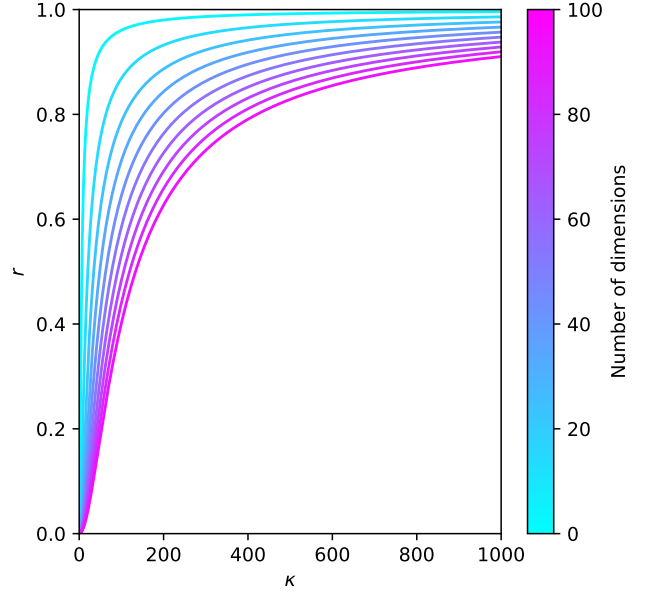


**Fig. 1.** We show hereabove the relation between the correlation coefficient between two fields in their Fourier representation  $r$  and the coefficient  $\kappa$  of the VMF distribution. This relation depends on the number of dimensions of the unit sphere.

a correlation likelihood between two vectors in  $p$  dimensions, is

$$V_p(\kappa) = \langle (\mathbf{x} \cdot \boldsymbol{\mu} - 1)^2 \rangle = \langle (\mathbf{x} \cdot \boldsymbol{\mu})^2 \rangle - 2 \langle \mathbf{x} \cdot \boldsymbol{\mu} \rangle + 1. \quad (16)$$

It can be computed with the similar trick as in Equation (9). After further manipulation of the properties of the Bessel function we arrive at the following relation:

$$V_p(\kappa) = \left( -\frac{p}{\kappa} \right) r(\kappa) + \frac{I_{p/2}(\kappa)}{I_{p/2-1}(\kappa)} (1 - r(\kappa)) + (1 - r(\kappa))^2. \quad (17)$$

We show in Figure 2 the relation between the square root of the variance, also called standard deviation, and the correlation rate for different numbers of dimensions and different correlation rates. As expected, the standard deviation decreases steadily when going from zero correlation to full correlation. We note that in the end the number of dimensions has a weak effect on this function. It is mostly present for the smallest number of dimensions. For a larger number of dimensions, the function can be well approximated by

$$V_p(\kappa) = (1 - r(\kappa))^2. \quad (18)$$

In Section 2.4, we further justify this approximation.

## 2.3. Extension of the distribution

In the previous section we have focused on the distribution using a maximum entropy argument and enforcing the first moment of that distribution. The problem, similar to Poisson distribution, is that the variance is set by the mean relation. We can extend the maximum entropy argument to derive another distribution that can enforce two constraints: the correlation rate and the typical fluctuation allowed according to that direction. We end up with

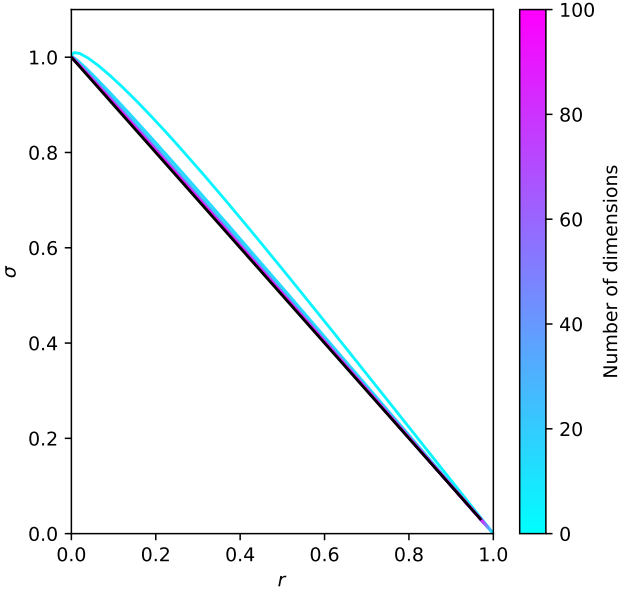


**Fig. 2.** Standard deviation from second moment of vMF distribution. This shows the typical width of the vMF distribution with respect to the considered direction.

an extension of the VMF distribution which takes the following form:

$$\mathcal{P}(\mathbf{x}|\boldsymbol{\mu}, \lambda_0, \lambda_1) \propto \exp\left(\lambda_0(\mathbf{x}\cdot\boldsymbol{\mu}) + \lambda_1(\mathbf{x}\cdot\boldsymbol{\mu})^2\right). \quad (19)$$

This function is a special case of the Fisher-Bingham distribution (Kent 1982). However, the normalization is much more complicated, and we defer the analysis of its advantages to future work. We focus here on the comparatively simpler von Mises-Fisher distribution.

#### 2.4. Small angle approximation

The VMF has a complicated normalization owing to its underlying non-additive space over which it is defined. However, it can admit small angle limits. Indeed we may expand the dot product in terms of the angle  $\vartheta$  between the given direction ( $\mathbf{b}$  in Equation (3) and (4)) and the random vector direction ( $\mathbf{a}$  in that same equation). This leads for the VMF to:

$$P(\mathbf{x}|\boldsymbol{\mu}) \propto \vartheta^{p-2} \exp\left(-\frac{\kappa}{2}\vartheta^2\right), \quad (20)$$

with  $\kappa$  the usual parameter governing the VMF distribution. Of course that distribution does not have anymore periodic properties.  $\vartheta$  in practice is related to  $\mathbf{x}$  and  $\boldsymbol{\mu}$  through:

$$\cos(\vartheta) = \mathbf{x}\cdot\boldsymbol{\mu} \quad (21)$$

We set the name of that distribution to  $P^\epsilon(\vartheta|\kappa)$ . To match the two distribution we again enforce the first moment of the distribution:

$$\int_0^{+\infty} d\vartheta P^\epsilon(\vartheta|\kappa) \left(1 - \frac{\vartheta^2}{2}\right) = r(\kappa). \quad (22)$$

This leads to the following simple equality:

$$r(\kappa) = 1 - \frac{p-1}{2\kappa} \quad (23)$$

We compare in Figure 3 the full VMF to the Gaussian approximation for a few values of  $\kappa$  and the corresponding dimensionality of the sphere. We show there the effect of using different, reasonable, correlation rate (series of colored line in each panel), and two dimensions of the space embedding the hypersphere (left and right panels). We see that the small angle approximation is in good agreement with the exact solution, though at  $r = 0.30$  the peak of the distribution is shifted and the tail at large angle is significantly shorter.

The advantage of working with the Gaussian approximation is that it is possible to introduce again the constraint that the variance of the distribution may fluctuate more than expected though at a smaller analytical cost.

In Section 2.2, we have noted that the variance of the direction seems well approximated with just  $(1-r(\kappa))^2$  (Equation 18). This can be understood from Equation (17) and (23). The asymptotic limits of the ratio of modified Bessel functions admit the following limits for any positive  $p$ :

$$\frac{I_{p/2}(\kappa)}{I_{p/2-1}(\kappa)} \underset{\kappa \rightarrow 0}{\sim} \frac{\kappa}{p} \quad (24)$$

$$\frac{I_{p/2}(\kappa)}{I_{p/2-1}(\kappa)} \underset{\kappa \rightarrow +\infty}{\sim} 1 \quad (25)$$

In the limits of large number of dimensions  $(1-r(\kappa)) \simeq \frac{p-1}{2\kappa}$ . We can then find two asymptotic approximations both for  $r \rightarrow 0$  and  $r \rightarrow 1$ . For  $r \rightarrow 1$ , we have:

$$V_p(r) \underset{r \rightarrow 1}{\sim} (1-r)^2, \quad (26)$$

further assuming that  $p$  is sufficiently large. For  $r \rightarrow 0$ , we have:

$$V_p(r) \underset{r \rightarrow 0}{\sim} (1-r)^2. \quad (27)$$

because the asymptotic limits of the first two terms are proportional to  $r$ . We thus have a function with similar asymptotic expansion at low and high correlation rate, as can be seen qualitatively in Figure 1. The typical allowed fluctuation for the direction is thus well determined by just  $1-r$ , for  $r$  sufficiently above 0, as seen in Figure 2.

### 3. Data model

In this work, we investigate the validity and resilience of a simple model to observations. In the next sections, we will rely on either perfect mock data, generated from that same model, or halo mock catalog, which exhibits more complex behavior. The data model that we adopt is the following. The deterministic model is assumed to generate a matter field from a white noise (also called ‘‘phases’’) by going through three transformations: a convolution by a scale invariant primordial spectrum, another convolution with a transfer function obtained with analytic approximation (Eisenstein & Hu 1998), and a final deterministic component. The final component may be obtained using Lagrangian Perturbation Theory, first or second order, or a full Particle Mesh with a limited number of time steps. As this step relies on a particle representation, we use a cloud-in-cell mass assignment to produce a regular mesh with the value of the matter density contrast.

The obtained mesh with the density contrast is directly provided to the correlation likelihood alongside the data projected on a mesh with the same size. We voluntarily omit to specify any tracer bias model. The correlation likelihood in practice absorb

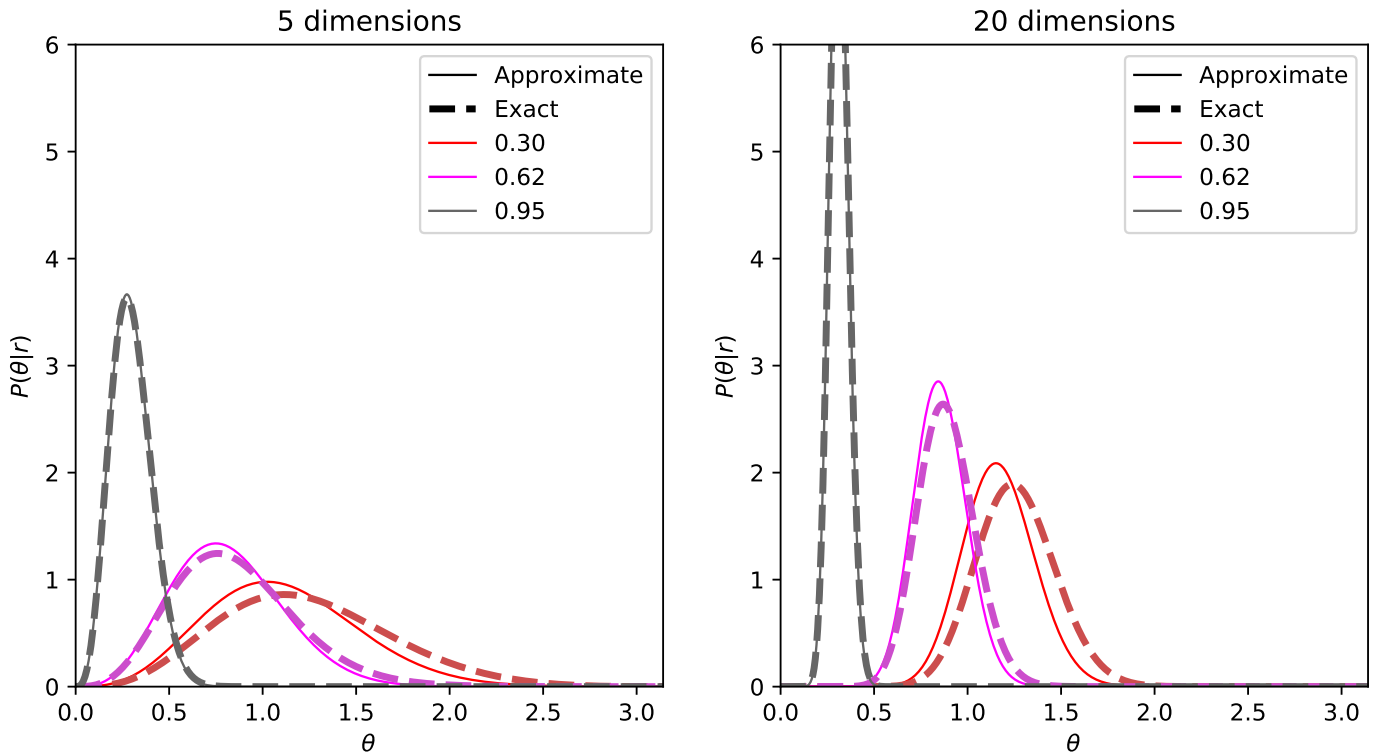


**Fig. 3.** Comparison of the effect of approximating Equation (6) by (20). The normalization is done independently for the two distributions, approximate (solid line) and exact (dashed line), and the relation between the correlation rate  $r$  and the parameter  $\kappa$  is applied with the specific relations of the two probability density distributions. The distributions are given for a few correlation rate ( $r = 0.30, 0.62, 0.95$ ) and two dimensions of the hypersphere ( $p = 5$  in the left panel,  $p = 20$  in right panel).

every systematic effect that looks like an arbitrary multiplication in the Fourier domain, provided the bins in  $k$  are sufficiently small. We exactly take this limit and, for the sake of the implementation, take a bin in  $k$  equal to  $10^{-4} h \text{ Mpc}^{-1}$ .

The last missing part is the correlation rate between those two fields for each  $k$ -bin. As we have seen in Section 2.2, equation (18), the correlation rate is directly, and simply, related to the level of noise fluctuations. Defining the rate is thus defining the precision of the model. We take it to be:

$$r(k) = \frac{1}{1 + (k/k_{c,1})^{s_1}} \frac{r_0 + (k/k_{c,2})^{s_2}}{1 + (k/k_{c,2})^{s_2}}, \quad (28)$$

with  $k_{c,1}$ ,  $k_{c,2}$ ,  $s_1$ ,  $s_2$  and  $r_0$  five constants that govern the shape of that function. This function has two components. The first one imposes that the correlation rate goes to zero at  $k \rightarrow +\infty$ . The second component allows the correlation rate to start from a value lower than one for  $k \rightarrow 0$  and increase to one asymptotically. This allows to mimic some of features observed in earlier work involving BORG reconstruction (Nguyen et al. 2021). We will see in practice that this behavior is in practice never adopted through inference from halo mock data (Section 5).

The test that we conduct here are run for a white-noise that is not sampled, i.e. it is fixed or, as it is sometimes said, “frozen”. Thus, it is still possible to jointly infer the shape of the correlation rate function  $r(k)$  and the cosmological parameter. This is an attempt to estimate the degree of reliability of the model from the correlation likelihood itself. The point of  $r(k)$  is to indicate to the likelihood for which scale the model should be trusted. The only anchor point for the likelihood to find the reliability is through the examination of high order statistics. Leaving that free for mass tracers for which the model of dynamics is not

well controlled is potentially dangerous, while the white noise is sampled. The danger comes from the coupling between the reliability and the cosmological parameters themselves. As an example, varying  $\sigma_8$  changes the effective time of collapse of structures, which changes the scale at which simple perturbation theory breaks down at low redshift. There is thus a degeneracy between  $\sigma_8$  and the scale at which the model breaks down. In principle, this could be lifted by a close examination of high order statistics but in practice we noted that the posterior probability always prefer to boost the correlation and induces systematic effect if it has the possibility to do so. It is thus safer to put a constant bound on the correlation rate for inference based on observational data, which indicates the absolute reliability of a model, as established by extensive tests within the standard model of cosmology. On the other hand, for the exercise conducted in this work, it is informative on the reliability of the simplified model to represent the complex dynamics of a full  $N$ -body simulation and structure identification. This in turn can help to produce the “safe” values for the correlation rate. We come back to this problem during the tests provided in Section 5.3.

#### 4. Self-consistent tests

With the data model that we have specified in the previous section, we aim now to validate the mock data generation and the inference algorithms. This test will not control whether the model is any good but whether the inferred posterior distribution is in agreement with the “ground truth”, which is the parameter used to generate the mock data. This section is subdivided in three parts. First, in Section 4.1, we provide an algorithm able to generate samples from the likelihood to generate the self-consistent

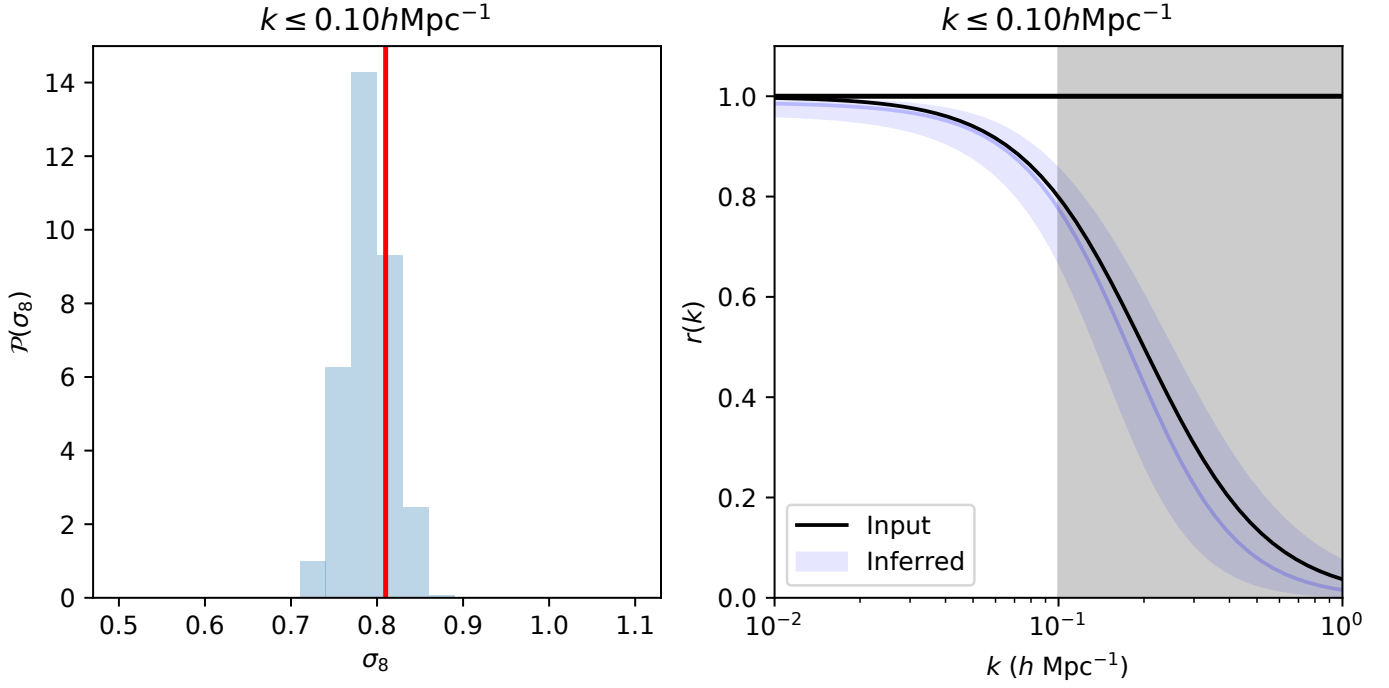


**Fig. 4.** Results of inferring the cosmological parameter and the correlation rate on mock data generated self-consistently from the data model of Section 3. We show in the left panel the normalized and histogrammed probability density distribution of the inferred value for the  $\sigma_8$  parameter alongside the one assumed to generate the data (vertical red line). Only large scales ( $k \leq 0.10 h \text{ Mpc}^{-1}$ ) were used in the inference. In the right panel we show the correlation rate that is jointly inferred: blue line is the ensemble average of the relation, while the shaded region is the region at one standard deviation. The black solid line shows the correlation rate function assumed to generate the mock data. The shaded grey region indicates the scales ignored for the inference.

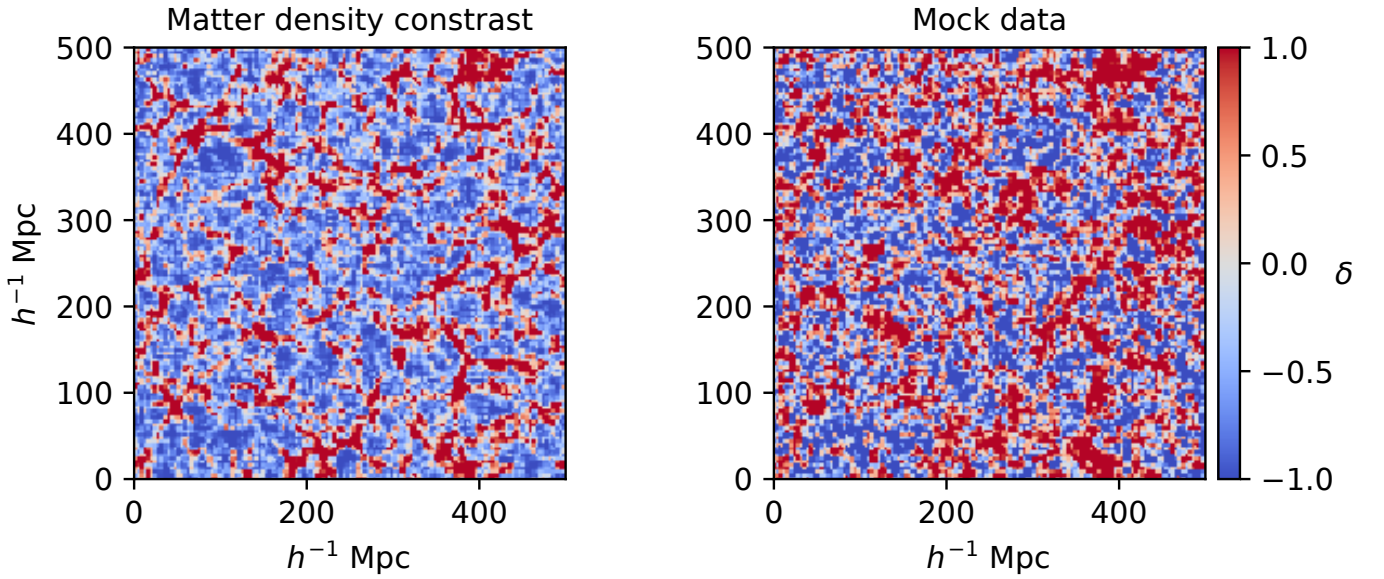


**Fig. 5.** Mock data used for the self-consistent test. The left panel shows the result of the cosmological simulation assuming the first order Lagrangian Perturbation Theory to evolve the density field, assuming the cosmology indicated in Section 4. The right panel is obtained by sampling mock data from the von Mises-Fisher distribution and conditioned on the field shown in left panel. We note that the features are indeed kept while noise is injected at small scales, as expected.

mock data. Then, in Section 4.2, we give the setup alongside a choice of the correlation rate function  $r(k)$ . Finally, in Section 4.3, we discuss the results.

#### 4.1. Algorithm to sample from the VMF

We need to sample an  $N$ -dimensional unit vector from the VMF distribution. We use a variant of the algorithm proposed in earlier work for specific directions (Kurz & Hanebeck 2015). The algorithm is derived from changing to the  $N$ -sphere coordinate

system ( $|x| = 1, \{\phi_i\}$ ). Without loss of generality, we can decide that  $\boldsymbol{\mu}$  is aligned with the first axis  $i = 0$ . In that case, the VMF in Equation (6) becomes:

$$f_p(\{\phi_i\}|\kappa)d^N \mathbf{x} = f_p(\mathbf{x}|\boldsymbol{\mu}, \kappa)J_\phi(\mathbf{x})d^N \Omega(\{\phi_i\}) \propto \exp(\kappa \cos \phi_0) \sin^{N-3}(\phi_0)d \cos \phi_0 d^{N-1} \Omega(\{\phi_i\}_{i=1..N-1}), \quad (29)$$

with  $\mathbf{x}$  constrained to be unit,  $|\mathbf{x}| = 1$ . Doing the usual change of coordinate  $\cos \phi_0 = w$ , we obtain that the parameters of the vector must be distributed as:

$$f_p(w, \{\phi_i\}_{i=1..N-1}|\kappa) = e^{\kappa w} (1 - w^2)^{\frac{N-3}{2}} U^{(N-2)}(\{\phi_i\}_{i=1..N-1}), \quad (30)$$

with  $U^{(N-2)}(\{\phi_i\})$  is the uniform distribution on the sphere of dimension  $N - 2$ . In practice we can generate a vector from that distribution, by sampling a Gaussian distributed vector in  $N - 1$  dimensions and normalize it to unity. We name this vector  $\mathbf{v}$ .

The second part of the distribution in Equation (30) is the distribution followed by  $\phi_0$ . Using the change of coordinate  $x = \cos \phi_0$  we transform the distribution as:

$$f_{VMF}(x; d, \kappa) = N_f(d) \times (1 - x^2)^{(d-3)/2} \exp(\kappa x). \quad (31)$$

$N_f(d)$  only depends on the number of dimensions and not on  $\kappa$ .

We generate a sample from  $f_{VMF}$  using the slice sampler algorithm (Neal 2003). We then synthesize the complete vector as follow. First we build a unit vector  $\tilde{\mathbf{z}}$  from the vector  $\mathbf{v}$  which is orthogonal to  $\boldsymbol{\mu}$ .

$$\tilde{z}_i = \frac{1}{\sqrt{1 + \mu_a^2 (\mathbf{v} \cdot \boldsymbol{\mu})^2}} \begin{cases} v_i & \text{if } i < a \\ -\frac{1}{\mu_a} \left( \sum_{i < a} v_i \mu_i + \sum_{i > a} v_{i-1} \mu_i \right) & \text{if } i = a \\ v_{i-1} & \text{if } i > a \end{cases} \quad (32)$$

And finally we build

$$\mathbf{z} = x\boldsymbol{\mu} + \sqrt{1 - x^2} \tilde{\mathbf{z}}. \quad (33)$$

The vector  $\mathbf{z}$  has unit norm, and is an i.i.d. sample from the  $N$ -dimensional VMF distribution.

#### 4.2. Generating an output with a specific cross-correlation limit

We use the algorithm shown in the previous section to generate mock data consistent with our likelihood probability distribution and deterministic dynamical model. For this test, and more generally in this work, we do not worry about masking and selection effect but whether the likelihood is able to survive the imprecision of the forward model. We adopt a box with a comoving side length equal to  $500h^{-1}$  Mpc, which has a total volume similar to the one of 2M++ (Lavaux & Hudson 2011). The initial and final mesh size is set to  $128^3$ . As indicated in Section 3, we use the first order Lagrangian Perturbation Theory as our basic benchmark. For the correlation rate we use the following parameter:  $r_0 = 1.0$ ,  $k_{c,1} = 0.2h \text{ Mpc}^{-1}$ ,  $s_1 = 2.0$ ,  $k_{c,2} = 4.0h \text{ Mpc}^{-1}$ ,  $s_2 = 1.0$ . They lead to the function represented with a black line in the right panel of Figure 4. We adopt a  $\Lambda$ CDM cosmology for a fiducial run, as provided by the Planck collaboration (Planck Collaboration et al. 2016):  $\Omega_m = 0.315$ ,  $\Omega_b = 0.049$ ,  $\Omega_\Lambda = 0.685$ ,  $w = -1$ ,  $n_s = 0.97$ ,  $\sigma_8 = 0.81$ ,  $H = 68 \text{ km s}^{-1} \text{ Mpc}^{-1}$ . We give in Figure 5 an example of such a field generated using the above parameter.

#### 4.3. Results of sampling the chain

We give in Figure 4 the two main results of the Monte-Carlo sampling of the chain. In the left panel, we give the inferred  $\sigma_8$  parameter and in the right panel the inferred correlation rate. In both cases, we provide the injected  $\sigma_8$  (left panel, vertical solid red line) and the injected correlation rate (right panel, black solid line). We note that the chain has achieved its goal of an unbiased inferred values of those two quantities, for a fixed white noise field. We also note that despite having completely removed the two point information of the final field and limiting the inference to large scales ( $k \leq 0.10h \text{ Mpc}^{-1}$ ), the constraints are still significant. Indeed, the inferred  $\sigma_8$  is  $0.790 \pm 0.026$ . This result is in line with an ensemble of other results obtained so far only with the bispectrum. They notably show that a huge amount of information is available in higher order statistics. The method that we propose here is a direct estimate of that amount of raw information. We also recover the correct correlation rate as indicated by the right panel of Figure 4, as well beyond the scales covered by the inference, though it is just a side effect of determining correctly the shape of that function at  $k \leq 10^{-1}h \text{ Mpc}^{-1}$ .

### 5. Tests on halo mock catalogs

In this section, we test our likelihood on more realistic samples of tracers which are based on the results of  $N$ -body simulations. In Section 5.1, we present the simulation setups. In Section 5.2, we analyze the impact of scale cut on the inference. In Section 5.3, we evaluate the impact of the model of dynamics on the correlation rate and the recovery of  $\sigma_8$ . We finish this study in Section 5.4 by considering tracers of different mass.

#### 5.1. Simulation setup

In this work, we use two  $N$ -body simulations with the same volume and cosmology but different mass resolution: one at  $512^3$  particle resolution, and the other at  $1024^3$ . The volume covered is  $(500h^{-1} \text{ Mpc})^3$  in all cases. The adopted cosmology is the same as the one given in Section 4.2. The  $N$ -body problem is evolved with GADGET-2 (Springel 2005) with force smoothing equal to  $1/50$  of the mean interparticle separation. We have used ROCKSTAR (Behroozi et al. 2013) to identify halos and sub-halos in these two simulations. We put a minimum number of particles at 10 (corresponding to  $M \geq 4.70 \times 10^{10} h^{-1} M_\odot$ , this is the default ROCKSTAR setting). In this work we make use of halos with a mass  $10^{12} h^{-1} M_\odot$  and higher ( $10^{13} h^{-1} M_\odot$  respectively) in the  $1024^3$  simulation ( $512^3$  respectively), corresponding to  $\approx 200$  particles, a number which is generally considered as safe (see e.g. Behroozi et al. 2013).

We choose to study two specific sub samples of the halo catalog generated that way, both mass selected:  $10^{13} - 10^{13.5} h^{-1} M_\odot$  and  $10^{12} - 10^{12.5} h^{-1} M_\odot$ . These are two standard regimes that are met in observations. The halos at  $10^{13} h^{-1} M_\odot$  are representative of halos hosting Luminous Red Galaxies (Ho et al. 2009; Zheng et al. 2009). The lower mass,  $10^{12} h^{-1} M_\odot$ , is representative of halos hosting Milky Way like galaxies (see a compilation by Wang et al. 2015).

#### 5.2. Effect of cutting in scales

In a first instance, we consider the effects of the truncation of information over spatial scale on the inference of  $\sigma_8$ . The results are summarized in Figure 6. In this plot we only consider

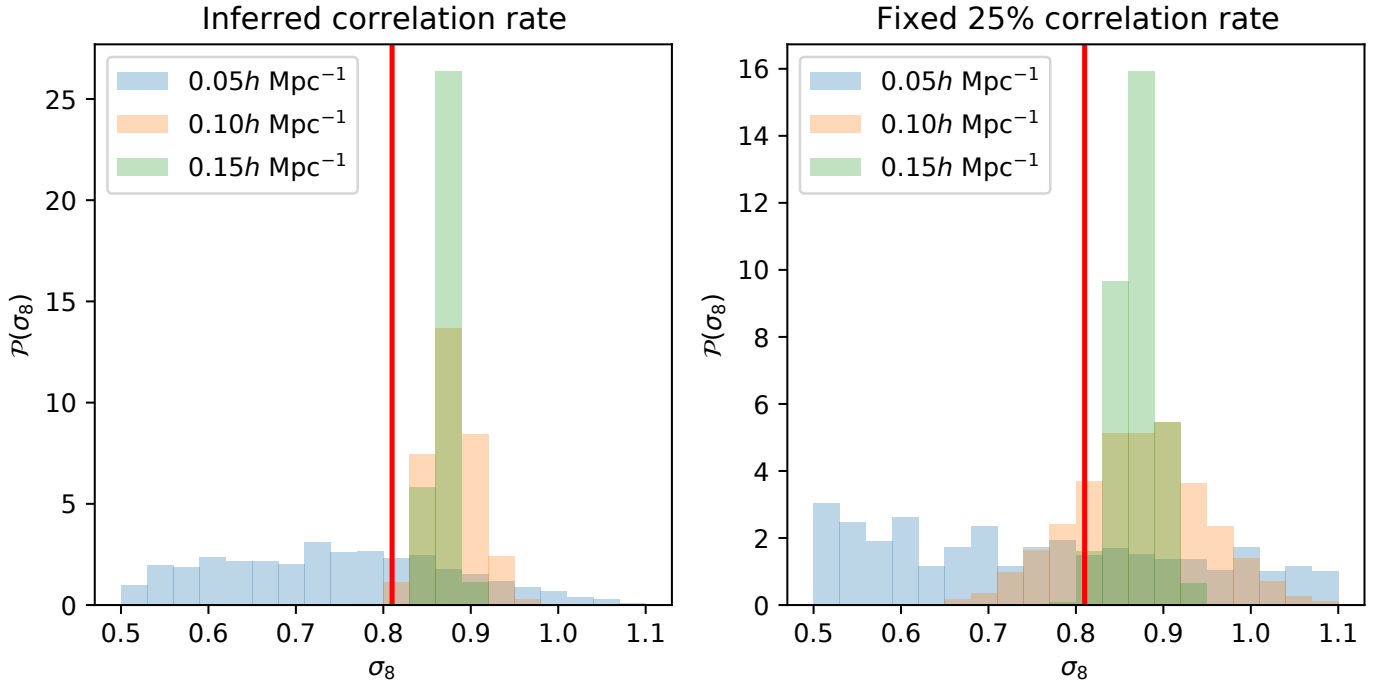


**Fig. 6.** Marginalized posterior probability distribution of  $\sigma_8$  for the halo mock catalog built from halos with mass inside the range  $10^{13} - 10^{13.5} h^{-1} M_\odot$ . We have assumed the first order Lagrangian Perturbation Theory to model the halo distribution. We show the result for different cuts of the Fourier domain  $k_c = 0.05h \text{ Mpc}^{-1}$  (blue),  $k_c = 0.10h \text{ Mpc}^{-1}$  (red),  $k_c = 0.15h \text{ Mpc}^{-1}$  (green). The  $\sigma_8$  used for the simulation is indicated with a vertical solid red line. We note that all distributions are qualitatively Gaussian distributed. The computation of the histogram has been limited for plotting to the range 0.5 – 1.1.

the halo mass corresponding to typically Luminous Red Galaxies, and we show the full shape of the posterior for each cut. As expected, for cuts at very large scales ( $k = 0.05h \text{ Mpc}^{-1}$ ), the posterior distribution of  $\sigma_8$  is broad, ranging from  $\sim 0.5$  to  $\sim 1.1$ . Interestingly, it is not completely uniform over this range and the peak of the distribution is roughly centered on the adopted value for the  $N$ -body simulation. We explain this by the fact that changing  $\sigma_8$  changes in practice the speed at which peaks cluster. Thus, it changes the higher order statistics in a non-trivial way. Our probability distribution is thus very sensitive to the statistics beyond 2-point correlation function, while that same function is completely ignored here. Increasing the cut to  $0.10h \text{ Mpc}^{-1}$  yields a very strong reduction of the width of the posterior distribution over  $\sigma_8$  by a factor  $\sim 10$ . We note that the peak of the distribution marginally overlaps with the assumed value for the  $N$ -body simulation. Some aspects of the full dynamics and halo distribution is thus correctly captured by first order Lagrangian Perturbation Theory. Increasing the cut  $k = 0.15h \text{ Mpc}^{-1}$  shows a consistent reduction of the width of the posterior, with the peak at the same location as for  $k = 0.10h \text{ Mpc}^{-1}$ . Despite this systematic effect of about 7%, we clearly see that higher order statistics holds a gold mine of information even at these very large scales. To give a related example, it was noted in [Hahn et al. \(2020\)](#) that the bispectrum holds a promise of reducing the error bar by a factor five on the mass of neutrinos.

To compare to a more realistic scenario for which the correlation rate will not be easily derivable (such as in observation), we run an experiment by fixing the level to a uniform 25% correlation rate. This level is much lower than the correlation inferred from the simulation for that same data-set (examples of such rates are given in the right panel of Figure 7). We see that the constraints have disappeared for the cut at  $k = 0.05h \text{ Mpc}^{-1}$ ,

while the two others are still very significant. The peak has not changed as expected as we increase the equivalent of the noise level uniformly. The PDFs have broadened to include the value of  $\sigma_8$  used for the simulation (shown with the vertical red line).

### 5.3. Effect of model of the dynamics

Having considered the impact of scale truncation, we now consider changing the model used to represent the dynamics of large scale structures. We focus on the first and second order Lagrangian perturbation theory, and a tCOLA  $N$ -body solver ([Tassev et al. 2013](#)). We choose to model the dynamics with only 5 time steps, and use a force resolution at twice the resolution of the particle grid. We show in Figure 8 a comparison of the inference on  $\sigma_8$  depending on the dynamical model adopted to generate the approximate dark matter density field. In that figure we jointly infer the correlation rate with  $\sigma_8$  without changing the white noise (i.e. keeping the “phases” fixed) from which the large scale structures are generated. We later consider in Figure 9 the impact of choosing a fixed correlation rate, set to 25%. Also, we will focus on the left panels of those two figures which correspond to the halos that may host a galaxy such as a Luminous Red Galaxy.

In the left panel of Figure 8, we show the impact of changing different gravity model and choosing different scale cuts  $k_{\text{cut}}$  on the inference of  $\sigma_8$ . Globally, the error bar reduces by a factor  $\sim 4$  between  $k_{\text{cut}} = 0.10h \text{ Mpc}^{-1}$  and  $k_{\text{cut}} = 0.20h \text{ Mpc}^{-1}$ , though the volume increases by a factor 8. A naive mode counting would yield a shrinkage of the errors by only a factor  $\sim 2.82$ . We note that at  $k_{\text{cut}} = 0.10h \text{ Mpc}^{-1}$  the measurement is within the inferred error budget. There are residual systematic effects in the cross-correlation lead that leads to a systematic in the infer-



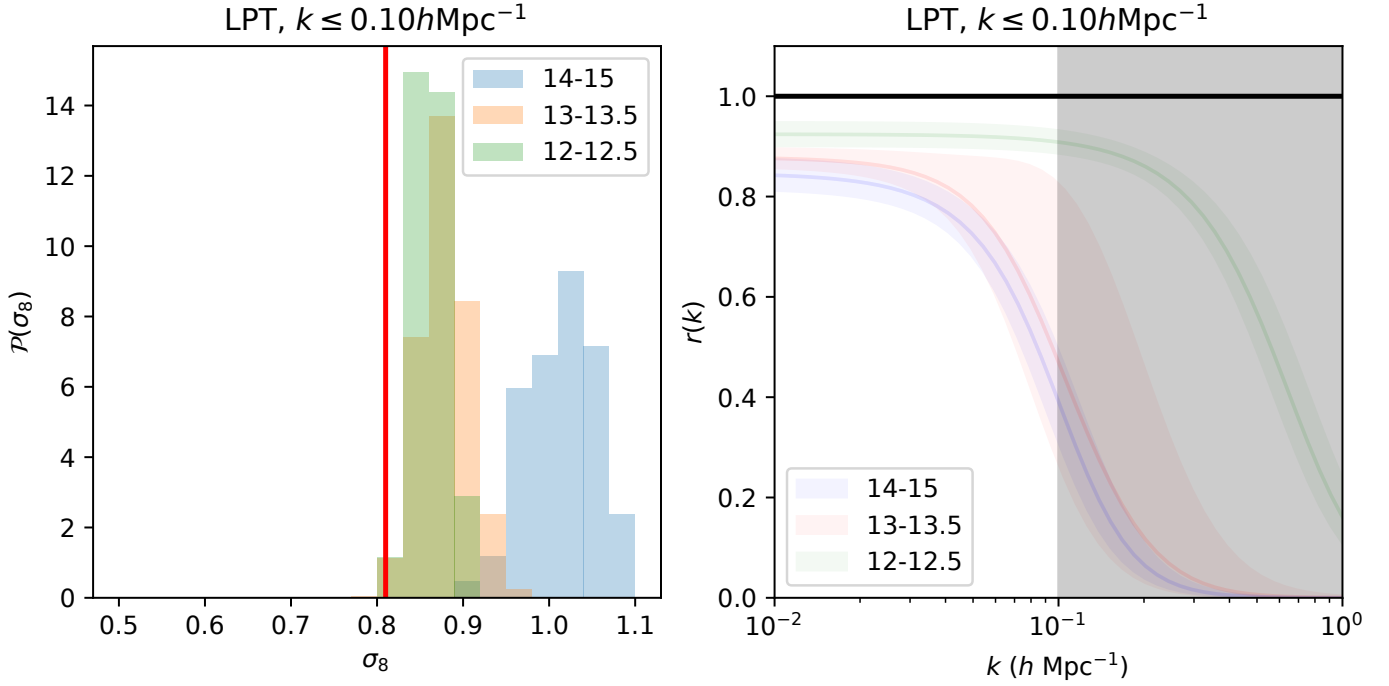


**Fig. 7.** Left panel: Posterior distribution for  $\sigma_8$  for different mass tracers and using the LPT dynamical model. Right panel: the jointly inferred correlation rate for different mode  $k$  with the shape as specified by the Equation (28).

ence of  $\sigma_8$  at the level of  $\sim 5\%$  with a  $5\sigma$  significance. Interestingly, the systematic is at its lower with the 2LPT model while tCOLA, despite having better higher order statistics for the dark matter field, is undershooting  $\sigma_8$ . Preliminary tests obtained by imposing a threshold on the matter field to mimic the effect of halo formation seems to improve the situation. More modeling is required though to improve on this. We note that the reduction of the error bar is similar for the three models of dynamics, indicating that the same higher order statistics must be involved. The way each model fail while increasing  $k_{\text{cut}} = 0.20h \text{ Mpc}^{-1}$ , which is still really large scales of  $\sim 30h^{-1} \text{ Mpc}$ , indicate that, even there, a significant amount of information must be present on the physics of dynamics of large scale structures. We also note that this is a regime that is also in principle sensitive to the physics of neutrinos (Lesgourgues & Tram 2011; Hahn et al. 2020; Palanque-Delabrouille et al. 2020).

In Figure 9, we further explore the impact of the model for dynamics but this fixing the correlation rate to 25%. As expected from previous section, the error bar is now quite larger. We have also less tension from the measurement obtained with the tCOLA model. For completeness, we tried with two simulations with different mass resolutions and different realizations of the initial conditions (labeled with “sim2”). Interestingly the effect of initial conditions is null for the 2LPT model while there is a  $1\sigma$  fluctuation for the tCOLA model. A systematic effect seems to be still present at  $k \sim 0.20h \text{ Mpc}^{-1}$  which we intend to investigate further in future work.

#### 5.4. Effect of mass of the tracers

In this section, we investigate the impact of using tracers of different mass on the result of the inference on  $\sigma_8$ . Lower mass tracer ( $M \simeq 10^{12}h^{-1} M_\odot$ ) are less biased than the one that we have studied so far in this work. Our expectation was thus that the measurement of  $\sigma_8$  would be globally in better agree-

ment with the value used for the  $N$ -body simulation. The results are shown through the comparison of left and right panels of Figure 8 and 9. We note that such a comparison was only possible for the higher resolution simulation for which halos of  $10^{12}h^{-1} M_\odot$  are resolved. The analysis jointly sampling  $\sigma_8$  and the correlation rate shows tightening of the error bars on  $\sigma_8$  as  $k_{\text{cut}}$  is increased. We would expect that tracers at  $10^{12}h^{-1} M_\odot$  to behave globally better than  $10^{13}h^{-1} M_\odot$  but that is not the case. They show at best the same level of mean systematics as for the higher mass tracers. This is slightly surprising given that they are supposed to be less biased and less affected by shot noise. On the other hand, their higher order statistics may be more complicated to describe. We intend to investigate this further in a future work.

## 6. Conclusion

This work presents a new approach to design likelihoods for large-scale structure analyses using concepts of linear cross-correlation analysis. By construction, it exhibits features to control the resilience of cosmological inference to uncertain noise and mis-modeling of the data. Notably, it is insensitive to scale-dependent galaxy biases, which is the usual way of modeling the relation between dark matter cluster and galaxy clustering. This biasing law is still subject to large modeling uncertainties. We note that simulating the dark matter distribution also automatically injects artificial numerical smoothing linked to the method used to solve the differential equations. One such example is the cloud-in-cell filter used to project particles to a mesh to be able to solve Poisson equation, or express dark matter distribution as a field on a mesh. Standard statistical analysis is made complicated by the procedure and may involve deconvolving the smoothing kernel. These defects do not exist by construction for the correlation likelihood as we are not sensitive to any linear, stationary, convolutional filter.

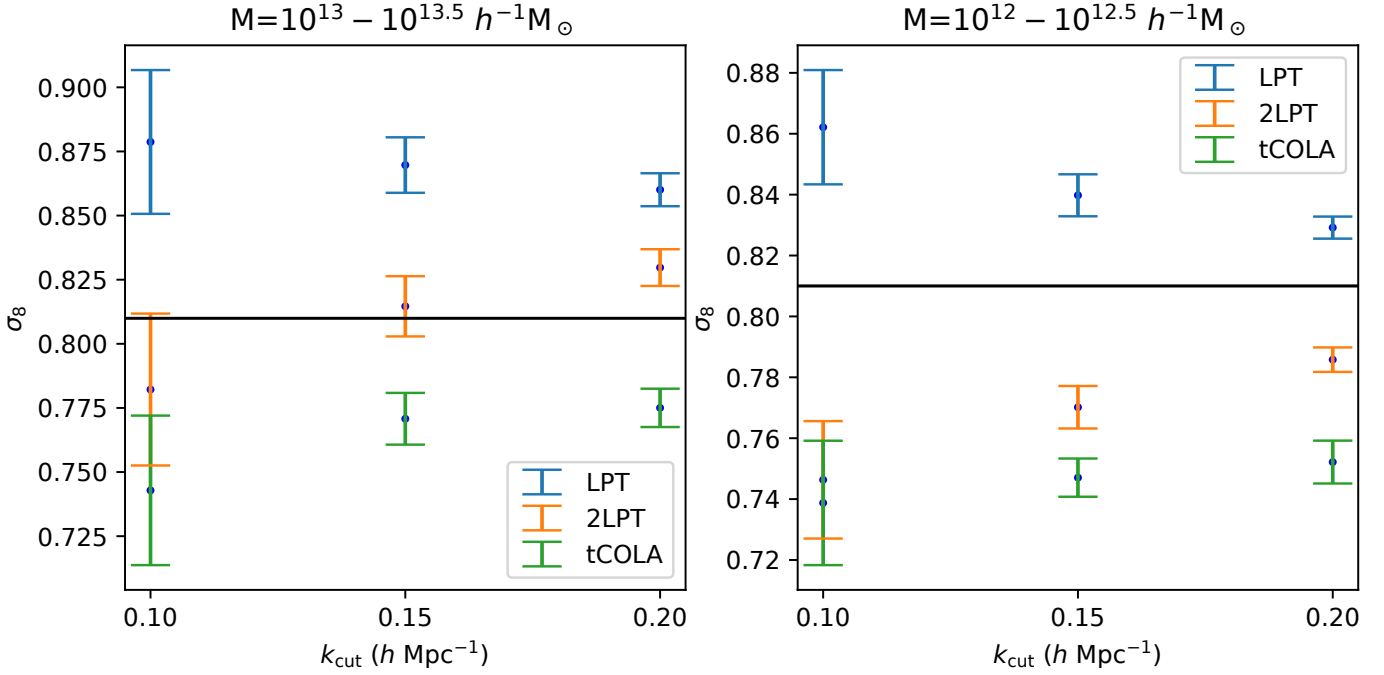


**Fig. 8.** Inference of  $\sigma_8$  for different choice of the dynamical model, truncation of the Fourier representation. The correlation rate is jointly inferred from the data, though assuming the shape function given in Eq. (28). Left (respectively right) panel presents the results for tracers with mass between  $10^{13}h^{-1} M_\odot$  and  $10^{13.5}h^{-1} M_\odot$  (respectively  $10^{12}h^{-1} M_\odot$  and  $10^{12.5}h^{-1} M_\odot$ ). In each panel we vary the assumed dynamical model: first order Lagrangian perturbation theory (blue), second order Lagrangian Perturbation Theory (orange) or a 5-time-steps t-COLA model (green). The result depend also on the modes used to make the inference, represented as the truncation  $k_{\text{cut}}$  on the X-axis.

This choice may be counter-intuitive with respect to the standard approach taken by the cosmological community. A lot of the statistical techniques rely on the 2-point statistics to extract cosmological information from observables. In this work, we have shown that even removing completely that information for the observation leads to sensitive measurement of the amplitude of that same statistics in the initial condition. Given the likelihood that we have used, we leverage information only from high-order statistics, and in that sense, our approach is complementary to probes usually adopted. This method could be very powerful in identifying and eliminate systematics in cosmological analysis.

Despite the simplicity of the proposed data modeling, there remains only a mild residual systematic uncertainty in the inference of  $\sigma_8$  at the level of  $1-2\sigma$  for halo catalogs that cover classes of galaxies such as Milky Way or Luminous Red galaxies, with a volume similar to  $2M++$ . We note that we may include non-linear biasing of tracers to improve on the present modeling. The linear correlation approach that we adopted here still allows for more complex bias models, which can correct the mismatch in the higher-order statistics that we have observed in this work. Such bias models may be, e.g., derived from differentiable machine learning methods (Zhang et al. 2019). It may also be provided by the framework of Effective Field Theory (Schmidt et al. 2019).

We intend to continue testing the limits of the cross-correlation likelihood, notably for initial condition generation in the context of the `borg` framework (Jasche & Wandelt 2013; Jasche & Lavaux 2019). As mentioned above, other extensions are possible to increase the robustness of the inference while keeping the complexity of the forward modeling small. One such extension is to enforce a minimal amount of fluctuation by setting the second-order moment, leading to the Fisher-Bingham

distribution. On the other hand, the forward modeling may also include non-linear transformation to increase the fidelity of the cross-correlation between the expected galaxy distribution and the actual observations. We expect the required corrections to be minor, which we intend to investigate in a follow-up publication. To conclude, we have proposed a new approach to designing likelihoods to make them robust to mis-modeling. We expect this development to enhance the confidence in inference results based on complex physical data sets, such as provided by extensive galaxy surveys.

*Acknowledgements.* This work was supported by the ANR BIG4 project, grant ANR-16-CE23-0002 of the French Agence Nationale de la Recherche. This work was granted access to the HPC resources of CINES (Centre Informatique National de l'Enseignement Supérieur) under the allocation A0020410153 made by GENCI and has made use of the Horizon cluster hosted by the Institut d'Astrophysique de Paris in which the cosmological simulations were post-processed. We thank Stéphane Rouberol for running smoothly this cluster for us. This work is done within the Aquila Consortium<sup>1</sup>. GL thanks Sebastien Peirani for providing with additional  $N$ -body simulation at high resolution. We acknowledge the use of the following packages in this analysis: Numpy (Harris et al. 2020), JAX (Bradbury et al. 2018), IPython (Pérez & Granger 2007), Matplotlib (Hunter 2007), Numba (Lam et al. 2015).

## References

- Allys, E., Marchand, T., Cardoso, J. F., et al. 2020, Phys. Rev. D, **102**, 103506
- Behroozi, P. S., Wechsler, R. H., & Wu, H.-Y. 2013, ApJ, **762**, 109
- Beutler, F., Seo, H.-J., Ross, A. J., et al. 2017, MNRAS, **464**, 3409
- Bradbury, J., Frostig, R., Hawkins, P., et al. 2018, JAX: composable transformations of Python+NumPy programs
- Cabass, G. & Schmidt, F. 2020, J. Cosmology Astropart. Phys., **2020**, 042
- Eisenstein, D. J. & Hu, W. 1998, ApJ, **496**, 605
- Elbaz, D., Cesarsky, C. J., Chaniai, P., et al. 2002, A&A, **384**, 848

<sup>1</sup> <https://www.aquila-consortium.org/>

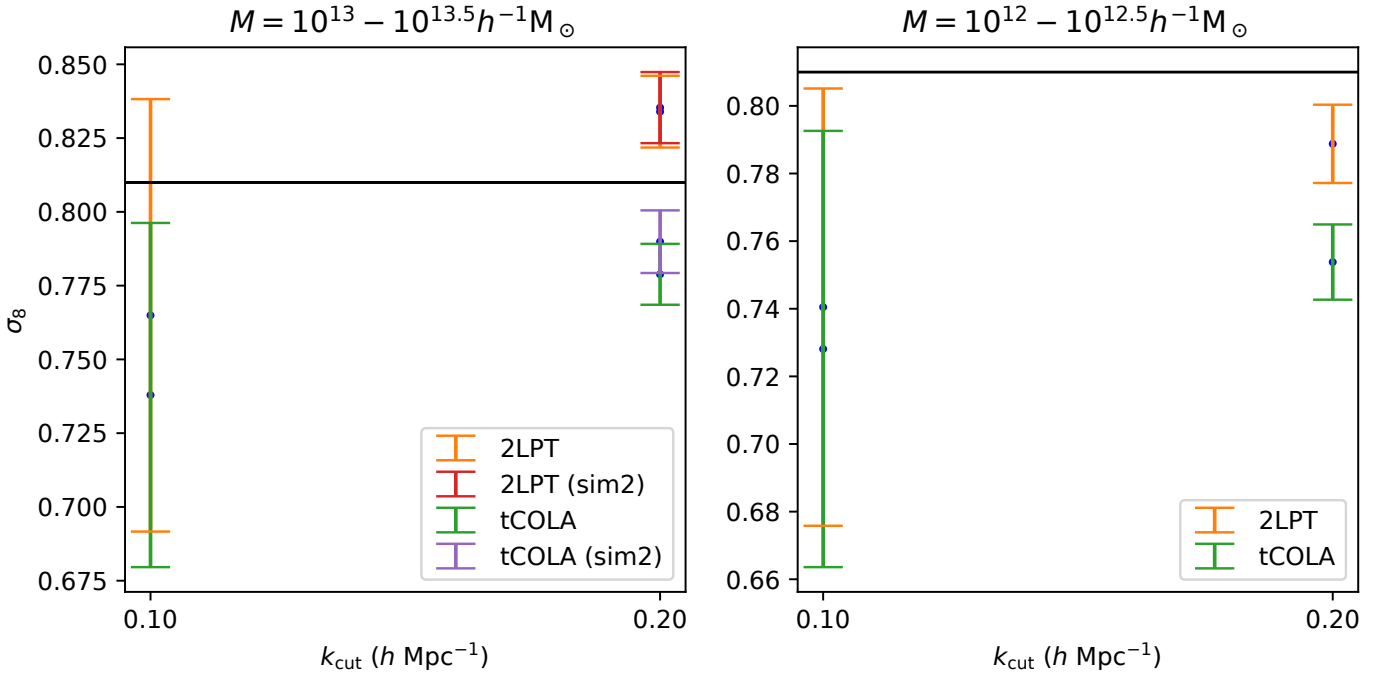


**Fig. 9.** Inference of  $\sigma_8$  for different choice of the dynamical model, for different choice of the truncation in Fourier representation, and for a *fixed* correlation rate of 25%. This differs from Fig. 8 for which the correlation rate was jointly inferred from the data. Left (respectively right) panel presents the results for tracers with mass between  $10^{13}h^{-1}M_{\odot}$  and  $10^{13.5}h^{-1}M_{\odot}$  (respectively  $10^{12}h^{-1}M_{\odot}$  and  $10^{12.5}h^{-1}M_{\odot}$ ).

Elsner, F., Schmidt, F., Jasche, J., Lavaux, G., & Nguyen, N.-M. 2020, *J. Cosmology Astropart. Phys.*, **029**

Fisher, R. 1953, Proceedings of the Royal Society of London Series A, **217**, 295

Granett, B. R., Neyrinck, M. C., & Szapudi, I. 2008, arXiv:0805.2974 [astro-ph] [arXiv:0805.2974]

Hahn, C., Villaescusa-Navarro, F., Castorina, E., & Scoccimarro, R. 2020, *J. Cosmology Astropart. Phys.*, **2020**, 040

Harris, C. R., Millman, K. J., van der Walt, S. J., et al. 2020, *Nature*, **585**, 357

Hildebrandt, H., Viola, M., Heymans, C., et al. 2017, *MNRAS*, **465**, 1454

Ho, S., Lin, Y.-T., Spergel, D., & Hirata, C. M. 2009, *ApJ*, **697**, 1358

Hunter, J. D. 2007, *Computing In Science & Engineering*, **9**, 90

Jasche, J. & Lavaux, G. 2019, *A&A*, **625**, A64

Jasche, J. & Wandelt, B. D. 2013, *MNRAS*, **432**, 894

Kent, J. T. 1982, *Journal of the Royal Statistical Society: Series B (Methodological)*, **44**, 71

Kurz, G. & Hanebeck, U. D. 2015, in 2015 Sensor Data Fusion: Trends, Solutions, Applications (SDF) (Bonn, Germany: IEEE), 1–6

Lam, S. K., Pitrou, A., & Seibert, S. 2015, in Proceedings of the Second Workshop on the LLVM Compiler Infrastructure in HPC - LLVM '15 (Austin, Texas: ACM Press), 1–6

Lavaux, G. & Hudson, M. J. 2011, *MNRAS*, **416**, 2840

Lesgourgues, J. & Tram, T. 2011, *J. Cosmology Astropart. Phys.*, **2011**, 032

Mead, A., Peacock, J., Heymans, C., Joudaki, S., & Heavens, A. 2015, *MNRAS*, **454**, 1958

Neal, R. M. 2003, *Annals of Statistics*, **31**, 705

Nguyen, N.-M., Schmidt, F., Lavaux, G., & Jasche, J. 2021, *J. Cosmology Astropart. Phys.*, **2021**, 058

Palanque-Delabrouille, N., Yèche, C., Schöneberg, N., et al. 2020, *J. Cosmology Astropart. Phys.*, **2020**, 038

Pérez, F. & Granger, B. E. 2007, *Computing in Science and Engineering*, **9**, 21

Planck Collaboration, Abergel, A., Ade, P. A. R., et al. 2014, *A&A*, **566**, A55

Planck Collaboration, Ade, P. A. R., Aghanim, N., et al. 2016, *A&A*, **594**, A13

Schmidt, F. 2021, *J. Cosmology Astropart. Phys.*, **2021**, 032

Schmidt, F., Cabass, G., Jasche, J., & Lavaux, G. 2020, *J. Cosmology Astropart. Phys.*, **2020**, 008

Schmidt, F., Elsner, F., Jasche, J., Nguyen, N. M., & Lavaux, G. 2019, *J. Cosmology Astropart. Phys.*, **2019**, 042

Schneider, A., Teyssier, R., Stadel, J., et al. 2019, *J. Cosmology Astropart. Phys.*, **2019**, 020

Smith, K. M., Zahn, O., & Doré, O. 2007, *Phys. Rev. D*, **76**, 043510

Smith, R. E., Peacock, J. A., Jenkins, A., et al. 2003, *MNRAS*, **341**, 1311

Smith, R. E., Scoccimarro, R., & Sheth, R. K. 2007, *Phys. Rev. D*, **75**, 063512

Springel, V. 2005, *MNRAS*, **364**, 1105

Sra, S. 2007, PhD thesis, Univ. of Texas at Austin

Tassev, S., Zaldarriaga, M., & Eisenstein, D. J. 2013, *J. Cosmology Astropart. Phys.*, **2013**, 036

van Daalen, M. P., McCarthy, I. G., & Schaye, J. 2020, *MNRAS*, **491**, 2424

van Daalen, M. P., Schaye, J., Booth, C. M., & Vecchia, C. D. 2011, *MNRAS*, **415**, 3649

Wang, W., Han, J., Cooper, A. P., et al. 2015, *MNRAS*, **453**, 377

Zhang, X., Wang, Y., Zhang, W., et al. 2019, arXiv:1902.05965 [astro-ph] [arXiv:1902.05965]

Zheng, Z., Zehavi, I., Eisenstein, D. J., Weinberg, D. H., & Jing, Y. P. 2009, *ApJ*, **707**, 554